### Title

Ion current and carbon monoxide release from an impinging methane/air coflow flame in an electric field




### Authors

Chien, Yu-Chien
Escofet-Martin, David
Dunn-Rankin, Derek



### Publication Date

2019-06-01

### DOI

10.1016/j.combustflame.2019.03.022

Peer reviewed

# Ion Current and Carbon Monoxide Release from an Impinging Methane/Air Coflow Flame in an Electric Field

Yu-Chien Chien*, David Escofet-Martin, Derek Dunn-Rankin

*Mechanical and Aerospace Engineering, University of California Irvine,*
*4200 Engineering gateway, Irvine, CA, 92697*

## Abstract

This research examines changes in the ion current and the release of carbon monoxide (CO) from surface-impinging coflow diffusion flames when subjecting those flames to high DC electric fields. Carbon monoxide results from the incomplete oxidation of hydrocarbon fuels and, while CO can be desirable in some syngas processes, it is usually a dangerous emission from forest fires, gas heaters, stoves, or furnaces where the core reaction insufficiently oxidizes the fuel to carbon dioxide and water. Electrical aspects of flames, specifically, the production of chemi-ions in hydrocarbon flames and the convective flows driven by these ions, have been investigated in ranges of application, and this research examines the use of electric fields as one mechanism for governing combustion as flames are partially extinguished when impinging on nearby surfaces. We evaluate the ion current and study the flame behavior at saturation current in response to the impinging plate location. We also measure the changes in CO emission, as correlated with variations in flame structure observed using OH chemiluminescence and OH planar laser induced fluorescence (PLIF), as a function of burner-to-plate distance and electrical potential applied to the flame. Three major saturation current impact regions in plate distance is observed, and it uses chemiluminescence with PLIF to illuminate the relative locations of the peak heat release zone and the extended oxidative zone changing by external electric fields. The results show that CO release correlates strongly with changes in location and extent of high concentration regions of OH in the surface-impinging diffusion flames. The results also show that electric fields affect the CO emission but that the burner-to-plate distance has the dominant influence. The detailed findings indicate that a continuous monitor of ion current from the flame to the impinging surface can be an effective sensing index of flame behavior and CO emission.

*Corresponding author.
*E-mail address*: chieny@uci.edu. (Y.-C. Chien)

*Keywords:* Electric field; Ion Current; Impinging Flames; Carbon monoxide; PLIF; Chemiluminescence

## 1. Introduction

Studies into the electrical aspects of combustion have a long and rich history that show how proper application of electric fields can act on the charge carriers in flames and modify combustion behavior including the effects of different orientation of electrode to the flow field geometries [1–9]. As a foundation, particularly in flame studies, the fundamentals of electrical aspects of combustion have been integrated and published by Lawton and Weinberg in 1969 [10]. Explorations in the use of electric fields for the manipulation and measurement of combustion, and efforts to understand the ion-driven wind transport and ion propagation in the thermal flow field are addressed as the key features of this research field. Research professionals, therefore, are trying to reveal and track the complex chemi-ion production and transport from different hydrocarbon flames with various fuel flow conditions, in a variety of combustor geometries and with several electric field influences (such as alternating/direct current or with various applied field orientations). Most of the research activities have been conducted on earth at 1g, but recent studies include investigations in the absence of buoyancy under microgravity and zero gravity combustion conditions [11–13]. These studies were designed to explore the keys of chemi-ion chemistry and ion driven winds, and they continue aboard the International Space Station (ISS) in the NASA Advanced Combustion via Microgravity Experiments (ACME).

The motivation for the current work has two components. First is the precursor exploration of electric aspects of flame quenching by Weinberg, et al. [14]. That research was focused on the prediction of incipient CO with electrical sensing. It revealed the possibility of using a low voltage source and different probe materials as a CO detecting sensor. The experiment employed low DC voltage from batteries (37 V and 56 V) and probed with an electrode around a partially premixed flame to observe the location of first ion current appearance. Reference [14] also postulated, however, that the source of CO release from impinging diffusion flames is the high concentration of partially oxidized fuel inside the flame envelope that avoids the final oxidation step. That observation suggested exploiting the flame shaping capability of an ion-driven wind [15] to control CO release from flames near a quenching surface. The second motivating component came from

the results of a related study of carbon monoxide (CO) release from flames near a quenching surface by Chien, et al. [16]. That work provided measurements of CO released from a small diffusion flame as a surface was brought into its proximity without any electric field being applied. By relating surface proximity to CO release, the study showed that the impinging surface plays a significant role in CO release because changes in the flow field change access of CO to hydroxyl, which then controls its oxidation to carbon dioxide. Therefore, finding the connection between electric field manipulation of a diffusion flame and changes in CO release with the flame-to-surface distance could be a useful contributor to the understanding of electrical aspects of combustion under near-wall quenching conditions. Hence, the main product of this paper is to observe and explain ion current changes and CO emission when a surface gradually moves close to a small diffusion flame, particularly under the influences of an electric field.

The literature of electric field effects in flames on carbon monoxide release from flames is limited, and even in those limited studies the range of electric field and flame configuration varies broadly. A recent review paper highlighting application in energy and process engineering of electric fields, along with plasma gasification, gives a comprehensive overview of the existing literature in the field [17] so the present article will focus on the literature of electric field effects on carbon monoxide. Here, we are further limiting the conditions to direct current electric field studies at a very low Townsend strength to avoid the complexity of corona discharge participation. Sepp et al. [18] measured the CO emission index (EI) from methane and propane diffusion and partially premixed flames. They observed the CO to have a reduction as 0-1kV was applied as an upward electric field from burner to downstream. The reduction rate was steeper as the mixture became fuel richer. Sakhrieh et al. [2] experimented on turbulent methane/air premixed flames with coflow up to 10 bar ambient pressure. They found that the CO concentration reduces with the increase of the downward field strength while a stronger upward field strength increases the CO concentration. Vega et al. [19] studied the emission from laminar premixed methane/oxygen/nitrogen flames with concentric polarities where the electrodes are parallel to the jet flow direction (instead of perpendicular). They found that the CO concentration decreased when

an inward electric field was applied. All of the above-existing studies are at different flow/flame conditions, comprising a premixed laminar flame, a turbulent flame, and an electric field applied from above or to the side of the flow stream. It is not surprising, therefore, that the results are independent and vary with each experiment. In addition, the variety in the studies makes it difficult to evaluate the physical process responsible for the electric field influence on the CO outcomes.

This current paper explores how the convective flow of an ion-driven wind near an impinging surface [20] affects CO release from flames, and the simplified geometry allows us to identify the major physical mechanisms involved. The research comprises measurements of the ion current, the reaction zone, the hydroxyl radical (OH) location, and the associated global carbon monoxide emission. We include schlieren imaging and OH* chemiluminescence, along with OH and CO planar laser induced fluorescence (PLIF) measurements, to elucidate the relationships between the reaction zone, major species fields, and the flow field that might account for the CO emission results with electric fields applied. We have already seen that when there is no electric field, the stagnating flow changes the OH distribution with the plate-to-burner distance, and this modification affects significantly the amount of CO oxidation [16]. We now examine if the application of an electric field has a similar influence. In addition, the work explores the possibility of detecting and changing the flame behavior electrically.

## 2. Experimental Apparatus

The experimental apparatus of this paper follows closely those of our previous study of carbon monoxide (CO) release from flames near an impinging surface [16] and our heat transfer study of electrical control of impinging diffusion flames [20]. Our diffusion flame is generated from a coflow burner with a 2 mm inner diameter (D) methane fuel tube with 37.7 ml/min fuel flow surrounded by a 25 mm diameter concentric air flow. Both the fuel and air are flowing at a nominal 20 cm/s mean flow velocity, with a fully developed parabolic profile in the fuel jet and a nearly top-hat velocity profile for the coflowing air. The 102 mm x 102 mm square steel impingement plate is located a variable distance (H) downstream from the burner exit. A DC high voltage power

supply (TREK, 609A-3) is used to produce the electric potential between the impinging plate and the grounded burner. Notice that in this work the electric field direction refers to the nominal electric field strength, where $E = -\Delta V/H$, with the negative sign included so that for a negative potential applied (i.e., potentials below burner ground) positive ions flow towards the impinging plate. In other words, the burner repels positive charges in a positive field. The upward/downward flow is equivalent to a positive/negative field strength respectively [20]. Voltage across a shunt resistor which allows electric current to pass through and monitors the ion current from the flame. The species measurement apparatus in this research includes the OH/CO PLIF approach followed as best practice [21–24] and CO gas analyzer measurements. This paper addresses substantive and key elements while further details of the method are covered in [16].

The OH PLIF measurements reported in this paper are conducted with a legacy laser system with manual tuning of the doubling crystals to find the region of the best performance of the equipment because the doubling crystals lack temperature control. The laser pulse energy is maintained below 1 mJ with a measurement sheet height 8 mm. Images are collected with a Phantom camera (v4.3) and a HiCaTT intensifier equipped with a P24 phosphor. The repetition rate is 10 Hz and for background luminescence suppression the images are taken with a 100-150 ns gate. The combination of Phantom camera and HiCaTT intensifier is also used for OH*, hydroxyl, natural chemiluminescence images. They are taken in the band from 300 nm and 340 nm, and they are recorded with a gate of 10 microseconds at a rate of 100 Hz. The tomographically reconstructed images [25] are processed from averaging 200 background filtered pictures to show a clear region of the reaction zone. Further details of the experiments are contained in the relevant subsections of the results section below. While the imaging quality of the OH/OH* produced from this legacy system is not as well-refined and smooth as that obtainable from more recent equipment with automated adjustments, the measurements here demonstrate effectively the trends of the OH distributions near the plate and the OH* identifies clearly the reaction zone in the impinging diffusion flames.

## 3. Results and discussion

### *3.1 Ion current measurement*

To determine the relationships between the electrical response and the effects of surface flame quenching on the electrical properties, the downstream plate is moved to different heights above the burner, and the voltage is swept across its full range for each height. The experimental results at each height include electric field strength (or voltage sweeps) up to the flame extinguishment or until a corona or arc discharge occurs. The range of the electric field at each height of the plate above the burner varies because the absolute distance between electrodes affects the voltage at which the flame extinguishes or an electrical arc breakdown is observed.

The ion current characterization experiment (or the development of the V-I curve) is conducted with plate heights from 12.5 to 1.5 H/D (25 mm to 3 mm in absolute distance). Figure 2a shows how the ion current changes with nominal electric field ($\Delta V/H$). The standard three distinct regions of the ion current response are apparent in the figure: sub-saturation, saturation and enhanced saturation (this latter is sometimes also referred to as secondary ionization or super saturation) [11]. A selection of flame images changing with impinging plate location and electric field is shown in Figure 3. The images within the red dashed box represent the flames within the ion current saturation region of the electric field. The images highlight that the flame reaction zone is not altered significantly by the electric field under saturation conditions, but that the flame is affected substantially in the region of electric field strengths producing enhanced saturation (outside of the dashed lines).

The ion current behavior at each height, figure 2a, shows that the field strengths at saturation stay close to each other with plate distance but that the voltage associated with the onset of enhanced ionization varies. An agreement has been observed particularly for positive field strength with mesh electrodes from an inverted jet burner [26], and the coflow burner with higher mesh electrode distances far downstream [27]. As the plate moves closer to the burner, the field strength

over which there is a saturation ion current increases; e.g., at H/D = 12.5, saturation spans from 1.7 kV/cm to 3.6 kV/cm, where for H/D = 1.5, saturation spans from 0.7 kV/cm to 4.7 kV/cm. The ion current response in the enhanced saturation region shows approximately parabolic behavior and a rapid current rise appears at higher plate location (as in the H/D = 12.5 case) that indicates an electric discharge arc as the field strength increases beyond breakdown.

Figure 2a shows that at the lower voltages the ion current increases with increasing field until it reaches a nearly constant value at saturation [11,12], and the limits, as expected, of the electric field become narrower as the gap between the plate and the burner decreases. Figure 2b shows a closer view of the transition from the sub-saturation to the saturation region. Since the fuel flow rate is constant, the decrease in the saturation ion current with electrode spacing indicates that the capability to generate ions decreases as the distance between the plate and burner decreases. In the far field flow cases from H/D = 12.5 to 6, the plate has not reached the visible flame zone so the saturation ion current changes little. As the plate moves down to the height of the unperturbed visible flame from H/D 5.5, the saturation ion current begins to drop consistently. The decrease of the saturation ion current at different electrode height appears to result from the flame reaction zone being interrupted and diverted by the impinging plate, which decreases the overall temperature, combustion completion, and reaction volume, thereby decreasing the ion production. The major ion dominant in the electrical aspects of combustion has been identified as the positive ion $H_3O^+$ produced in the reaction zone of hydrocarbon flames [10,28]. Figure 2 also highlights that the electric field strength to achieve saturation is nearly constant with plate height for a negative field and burner-directed ion wind. It is around 0.25 kV/cm, except for the lowest heights where the field at saturation is closer to 0.4 kV/cm. At the same time the nominal electric field strength to reach saturation with a positive field and burner-directed ion wind is higher in all cases than those with a negative field, and for the positive field case the electric field strength at the onset of saturation decreases steadily with decreasing H/D.

Figure 4a plots the saturation ion current from Figure 2 for positive and negative field strength at each impinging plate height per volumetric flow rate of methane, from the plate-to-burner

distance (H/D) 1.5 to downstream 12.5. The figure shows that the saturation ion current at the same impinging plate height is always higher for the positive field, and even though the difference decreases with decreasing H/D, the current is not equal, even at the lowest plate location. The saturation current for positive field and negative field reaches an asymptotic maximum at distances (H/D > 7; positive field, and H/D > 10; negative field) where the flame is far away from the impinging plate.

Another difference between positive and negative fields is that the ion current reaches the unperturbed level of saturation (i.e., distant plate condition) faster with the plate increasing distance on the positive side as compared to the negative side. This behavior is shown more directly in Figure 4b, which normalizes the current based on the peak saturation ion current for each polarity respectively in order to give a full scale of comparison. The slope of the normalized saturation current is steeper for the positive field than for the negative field, reaching a maximum sooner, with 35% wider full current range distributed at all heights. The plate distances where the saturation current ($i_s$) reaches within 5% of the maximum saturation ion current ($i_{s,max}$) are 4.5 H/D for positive field and 6 H/D for the negative field.

The ion current measured here can be also described using the construction of multiple zones of resistance in series from one electrode (plate) to another (burner). The inter-electrode space contains different zones, illustrated in Figure 5a, as addressed in Weinberg et al. [14]. Notice that Figure 5 uses a 2-D flame, therefore, the actual size of the four zones is changing along with the flame geometry. The dashed boxes only demonstrate the concept. The reaction zone and the hot product zone where the ion generation occurs, and where charge attachment/exchange or clustering occur have major influence over other zones. The electric potential ($V$) required to remove all the ions from the reaction zone (i.e., the voltage at the onset of saturation) can provide some key information to understanding the coupling effect between these two zones.

The voltage and the electric field strength applied to the impinging plate when the system just reaches the point where the ion current saturates is plotted versus plate height in Figure 6a. Figure 6a shows that the saturation potential increases along with the distance increase between the

electrodes and is more significant for positive field than for negative. The change of saturation voltage, shown in Figure 6b, between plate heights when the electrode is situated far downstream is enhanced. This implies, for both polarities, that the space charge needed to reach saturation is amplifying with H/D increase. This can be observed in Figure 6b, from H/D = 6 to 12.5, where the plate is beyond the visible flame height 10 mm (H/D = 5.5). In this case, the saturation potential over the distance between the electrodes changes from 1.1 to 1.7 kV/cm for the positive field while there is almost no change for the negative field.

At these distances (H/D > 6) where the flame geometry, particularly the reaction zone, is unperturbed by the plate, the ion removal reaches the formation rate, which remains at the same level, as can be seen from the asymptotic region of the saturation current (Figure 4) for each polarity. In the positive field case, the upward ion driven wind helps keep the reaction zone compact and facing inward. This maintains the very similar ion formation within the reaction zone but with a thicker hot production region leading to positive ions moving toward the plate electrode with an extended path over the inter-electrode region. This increase of traveling length reduces the conductivity (or increases the resistivity) from the reaction zone to the plate electrode causing a reduction of current density if the voltage remains the same. The space charge is required to keep up with the current density change as the H/D increases, and in order to maintain the saturation potential across the reaction zone, the total voltage applied must increase [10]. This phenomenon for the negative field case has nearly no influence because the positive ions are moving toward the burner electrode with very similar trajectory at the same distances. For both polarities, the negative charges are primarily electrons moving opposed to positive ions; they are traveling from the reaction zone toward one electrode through the high voltage charge circuit and recombining with the positive ions at another electrode as governed by the ion formation rate. The electrons special characteristic of high mobility, which is 2-3 orders of magnitude larger than for the positive ions, means that their concentration is low in the interelectrode space [29]. The resistance at saturation, $R_s$, between the electrodes, and the resistance over the distance, $R_s/H$, are deduced from the

saturation voltage divided by saturation current, and are as shown in Figure 7a and 7b as a function of H/D.

In the region of 4.5 < H/D < 5.5, where the impinging plate just starts touching and influencing the flame, and where the saturation current starts changing but is not yet changing significantly (Figure 4), the saturation voltage over length ($\Delta V/H$) and saturation resistance over length ($R_s/H$) remain unchanged (Figure 6b, 7b) while the saturation voltage and resistance are both decreasing with the decreasing ion current (Figure 6a, 7a). This result indicates that the hot product zone is very thin and is no longer in charge of the overall current response. The impinging plate attracts positive ions immediately from the reaction zone without going through a thick layer of the hot gas, so at these plate heights the ion current is dominated by ion formation directly. Among these heights, there is relative subtle change in saturation voltage and resistance for the negative field case but the trend can still be observed.

At small plate distances, H/D < 4, the saturation current, voltage, and resistance tend to converge toward each other for both polarities. This convergence indicates that the impinging plate is gradually more dominant in controlling the overall combustion physics. This dominance does not rely on the heat loss from the impinging plate because the overall heat flux to the plate changes little with changes in the electric field [20]. The plate position influence on ion production occurs because, even at the same fuel/air velocity, the impinging plate expands the reaction zone, which influences the reaction rate (Figure 3 or [16]). The schlieren imaging results in [20] demonstrate that the negative field produces a broader hot gas stagnation plume as compared to the positive field, but this effect is less pronounced at the lowest plate location (H/D = 1.5). This means that the plate position affects the flame by generating a smaller formation rate and saturation current as the H/D reduces from 4 to 1.5, as is seen in Figure 4a. The linear fit at these lower plate heights in Figure 4a shows that the saturation current change rate for the positive field is many times higher than for the negative field with plate distance. This means that the ion formation is vigorous for the positive field because of the encouragement of additional ion production from the ion wind. This is visible with the very similar reaction geometries observed from the natural flame images

and OH* for different electric fields but small plate spacing (Figure 9). From Figure 6b, the saturation voltage over length for positive fields reaches its lowest value at H/D =1.5, while the negative field shows the highest saturation voltage, though the difference between the two polarities of saturation voltage is smallest at this condition.

In the positive field system in the close plate region (H/D < 4), the effective flame resistance is nearly constant while both the saturation current and saturation voltage vary (Figure 4a, 6a). The gas from the stagnation flow is directed along the plate and releases immediately with very short residence time and the positive ions are flowing directly to the plate over a very small gap. The space charge needed in order to separate ions from the reaction zone is decreasing because of this close-plate interaction. This leads to the observed decrease of the saturation voltage over length ($\Delta V/H$) and fairly constant effective resistance over length ($R_s/H$) with the reducing plate distance (Figure 6b and 7b).

For negative polarity, at these small plate distances, since the overall change of saturation current is small, and the saturation voltage or the saturation resistance almost remains at the same level, evaluating the saturation resistance over length and the saturation voltage over length is not an effective comparison. It is worth noticing that the saturation ion current changes (but very little) under the influence of a negative field with the plate distance decreasing, and the saturation voltage/resistance maintaining itself at a similar value implies that the positive ions are moving toward the burner easily with constant space charge between the electrodes, and with the high flexibility of the electrons traveling downstream.

The overall saturation current, saturation voltage and resistance for the positive field is always larger than for the negative field. The reason for this polarity asymmetry is very complicated because the saturation ion current is controlled by flame character such as burning rate and temperature resulting from the combination of electric body force coupling with buoyancy force. Saturation voltage is affected by the space charge distribution, and the mobility and number density of charge carriers are responsible for delivering the current that must be overcome to create a charge separation within the flame reaction zone. The effective resistance is the ratio of these two

properties not only considering the reaction zone but also the hot gas product region at different plate distances. It is not yet possible to elaborate on the detailed processes with the experimentally available information, especially under the constant buoyancy force coupling with momentum driven by the ions in the electric field.

To conclude, there are three categories of influence that the impinging plate produces for the saturation current between the inter-electrode region of a laminar coflow flame; the hot gas product zone dominant region at higher plate distance (H/D > 6), the reaction zone dominant region near the flame height (4.5 < H/D < 5.5), and the stagnation flow dominant region at small plate height (H/D < 4) when the plate has already interfered substantially with the flame.

If we now consider that the saturation ion current correlates with combustion efficacy (i.e., temperature and heat release), the normalized magnitude of the saturation ion current can be used to track the influence of the stagnation plate on the CO release. As mentioned earlier, the saturation ion current decreases with H/D, reflecting in part incomplete combustion which also leads to carbon monoxide release (i.e., fewer ions are formed in the smaller less robust reaction zone). To test this hypothesis, carbon monoxide was monitored from flames under the influence of the impingement plate and an electric field.

*3.2 CO measurement*

The quantitative measurement of CO emissions with a gas analyzer (TSI CA-CALC 6200; accuracy 1 ppm CO) from the flame under the influence of different fields is shown in Figure 8a, with H/D from 3.5 to 1.5, which are the heights where we have significantly higher (more than 5 times) CO release than from the unperturbed diffusion flame with no electric field applied (i.e., over 100 ppm - Emission Index 28 g/kg). The results are normalized to the steady concentration for the coflow flame without a plate influence and without any electric field, which is approximately 120 ppm [16]. We measure the carbon monoxide by taking a representative well-mixed sample from the flame surroundings in the chamber in steady state. Thus, the CO influx

from the flame matches the CO outflux from the containment chamber, allowing a reliable assessment of the CO released by the flame to the surroundings. The CO results are focused on the relative effects of plate impingement so the data are shown in a form that is normalized to the CO concentration achieved in the chamber from a flame unaffected by the plate. Our prior work has shown that our unperturbed flame effectively produces approximately 120 ppm CO, with an emission index (EI) of 5. The uncertainty in the measurement at each point is less than the size of the data point marker.

Figure 8 shows that as the negative field strength increases, the CO level rises. On the positive field side, CO does not show a consistent nor significant change with the electric field but, except for the closest plate location, the concentration still grows slightly and reproducibly just before falling near the breakdown or extinguishment limit. The effect on the negative side can be explained because the downward directed ion driven wind affects the flow field similarly to moving the quenching plate slightly closer the burner, which allows the flame to release more unreacted CO. At the same field strength applied, CO increases with closer plate spacing. The effect on the positive side is more complicated. It may relate to unsteady fluctuations in the combustion process driven by the electric field or to the fact that drawing the flame upward brings the reaction zone closer to the plate, increasing the heat loss. There are then competing effects of the CO release and OH formation near the plate that are difficult to assess separately. However, as the later presented PLIF and chemiluminescence results show, the effects on the OH distribution from the plate interference with the flow field and flame are larger than are those from the electric field driven ion wind.

Figure 8b shows the CO results normalized to the respective plate height but zero-field condition. This normalization indicates that both positive and negative fields can adversely affect CO release from impinging diffusion flames. The normalized picture shows generally that as the negative field and the downward directed ion driven wind grows, the CO level rises. In order to

understand some of the phenomena responsible for these CO results, the following measurements describe the flame location, as indicated by OH* chemiluminescence, and the reactive OH location as shown from planar laser induced fluorescence.

*3.3 OH*/OH PLIF*

The OH PLIF measurements are conducted using an $Nd^{+}$:YAG laser with doubling crystals followed by a dye laser emitting light at 283 nm to reveal OH fluorescence in the flow. Natural OH chemiluminescence emission from the flame reaction zone is collected with a band pass filter from 300-340 nm representing the reaction zone, and from this information the flame contour is tomographically reconstructed. Figure 9a shows the OH PLIF signal (colored) and tomographically reconstructed OH* chemiluminescence (grayscale), and 9b is a combined image. The color bars next to the image help show the relative intensity change for both signals. Note that the extent of the laser sheet in both of the OH and CO PLIF measurements domain is H/D =2 below the impinging plate, and the experiment is performed without taking the vignetting effect of the plate into account [30]. The measurements are conducted at each height with the zero field condition and the two highest electric field strengths first, and then alternating polarity first and reducing field strength second.

The results show that the overall OH fluorescence intensity decreases as the plate approaches the burner. This decrease of strength is a combined effect from the decreasing mole fraction of OH, the temperature dependence of the transition $Q_1(7)$, the density changes due to temperature variation, vignetting as the plate height changes, and collisional quenching. With all of these effects, the results provide primarily comparative information, but the integrated use of fluorescence and tomographically reconstructed chemiluminescence can identify the heat release (HR) zone [31] and at the same time track the primary combustion location [32]. The periodic structure of the fluorescence results from a non-uniform laser sheet with effective measurement height H/D=2 below the plate. The results concentrate in the near plate region to demonstrate the

geometry and distribution of the target species (OH) particularly where the effects of the plate and the electric field driven ion wind are greatest.

One clear comparison of these OH images show that the OH distribution change with electric field at the flame tip near the plate is more affected by the negative field at the H/D=3.5 compared to H/D=2.5, which correlates in Figure 8 with the higher relative CO emissions. The indirect relationship between OH fluorescence strength and location resulting in variations of CO emission is strengthened with direct measurements of CO near the impinging plate for the different flame cases, as seen in Figure 10.

*3.4 CO PLIF*

The CO planar laser induced fluorescence measurement method follows the best practice of two-photon excitation with a pulsed laser, and the wavelength used is 230.034 nm. The details have been described in [16]. The very thin layer of bright CO fluorescence right below the impinging plate at the quenching zone is due to the low plate temperature increasing the CO signal, combined with the increased density. The temperature where the OH exists (which is located surrounding the reaction zone) is farther from the plate and less affected by the steep temperature gradients near it [16]. Figure 10 shows the result of CO PLIF with changing electric fields. The CO signal near the plate did not appear until the plate height lowered to H/D 4.5, and there was no CO fluorescence detected at H/D 5.5.

The OH and CO PLIF measurement results show that OH fluorescence changes with the electric field, distributing outwardly with negative fields and gathering toward the axis with a positive field. At relatively high plate-to-burner spacing the electric field has a minor influence on the OH PLIF intensity but it does affect the location of the OH as the fields change the position of the flame sheet. When a positive field is applied, the ion driven wind pulls the flame in the direction of the flow field and the reaction becomes vigorous toward the plate. OH distributes strongly near the plate and less CO is left within the flame. At closer plate distances the field affects the OH intensity

as well as its position/orientation. With negative fields, the positive ions produce a downward blowing wind that causes the reaction sheet to broaden, which creates a flow path for the gas inside the flame sheet to follow that avoids interaction with the OH radical. Even though the heat release (HR) zone is mostly unaffected, the redirection allows CO to escape with the stagnation flow. In this work we are using the OH chemiluminescence as a measure of the heat release zone. In H/D = 3.5, there is the most dramatic effect of the electric field as regards the magnitude of OH fluorescence but there is little change in OH location/distributed orientation relative to the flame sheet. These results reflect that changes in CO rely heavily on contact with OH [16], and the structural alteration conveys that CO can avoid oxidation and escape along with the stagnation flow.

## 4. Conclusion

This paper helps describe the relationship between ion current, flame shape, and CO emission when a coflow impinging non-premixed flame is influenced by an external electric field. It describes particularly the spatial relationship between the reaction zone and heat release zone with quenching in small diffusion flames, and how the relationship can affect saturation ion current as well as CO release. There are four components in the findings of this research: (1) it describes the electric field effects, particularly on the ion current and the fundamentals of how the flame responds to the impinging plate; (2) it elaborates on how three major factors influence saturation current for different impinging plate distances, (a) hot product dominant (b) reaction dominant (c) stagnation flow dominant, by correlating ion formation with saturation ion current, saturation voltage and resistance for different plate locations; (3) it demonstrates the role of the stagnation flow and the ion-driven wind in carbon monoxide release with variations in burner-to-plate location; and (4) it provides information on the role of the OH changes with electric field and plate-to-burner distance. It shows that OH location and concentration during flame quenching correlate strongly with carbon monoxide release, and that plate location has an even larger effect on the OH than does the electric field. The impinging plate plays an important role in ion current response by

affecting the flame's shape, flow direction, reaction conditions, and the ion distribution with respect to the electric field. Additional investigation into how the saturation current correlates to CO release rates with plate location, and numerical simulations to help trace ion concentrations and pathways can definitely further refine these findings. The data provided is a comprehensive set, spanning a range of conditions, and providing a consistent geometry, to determine the links between electrical sensing and forcing in impinging flames.

**Acknowledgements**

This work is supported by NASA's ISS Research Project via agreement NNX11AP42A with Dennis Stocker as Technical Monitor. The authors would also like to acknowledge the contributions of Koji Yamashita from Aoyama Gakuin University.

**References**

[1] H.F. Calcote, Electrical Properties of Flames: Burner Flames in Transverse Electric Fields, Symp. Combust. Flame Explos. Phenom. 3 (1948) 245–253.
[2] A. Sakhrieh, G. Lins, F. Dinkelacker, T. Hammer, A. Leipertz, D.W. Branston, The Influence of Pressure on the Control of Premixed Turbulent Flames Using an Electric Field, Combust. Flame 143 (2005) 313–322.
[3] S.H. Won, M.S. Cha, C.S. Park, S.H. Chung, Effect of Electric Fields on Reattachment and Propagation Speed of Tribrachial Flames in Laminar Coflow Jets, Proc. Combust. Inst. 31 (2007) 963–970.
[4] J.D.B.J. van den Boom, A.A. Konnov, A.M.H.H. Verhasselt, V.N. Kornilov, L.P.H. de Goey, H. Nijmeijer, The Effect of a DC Electric Field on the Laminar Burning Velocity of Premixed Methane/air Flames, Proc. Combust. Inst. 32 (2009) 1237–1244.
[5] M. Karrer, M. Bellenoue, S. Labuda, J. Sotton, M. Makarov, Electrical Probe Diagnostics for the Laminar Flame Quenching Distance, Exp. Therm Fluid Sci. 34 (2010) 131–141.
[6] J. Schmidt, B. Ganguly, Effect of Pulsed, sub-Breakdown Applied Electric Field on Propane/air Flame through Simultaneous OH/acetone PLIF, Combust. Flame 160 (2013) 2820–2826.
[7] P.R. Salvador, K.G. Xu, Electric Field Modified Bunsen Flame with Variable Anode Placement, J. Thermophys. Heat Tr. 31 (2017) 956–964.
[8] Y. Xiong, D.G. Park, B.J. Lee, S.H. Chung, M.S. Cha, DC Field Response of One-dimensional Flames Using an Ionized Layer Model, Combust. Flame 163 (2016) 317–325.
[9] D.G. Park, S.H. Chung, M.S. Cha, Visualization of Ionic Wind in Laminar Jet Flames, Combust. Flame 184 (2017) 246–248.
[10] J. Lawton, F.J. Weinberg, Electrical Aspects of Combustion, Oxford University Press, London, 1969.
[11] M.J. Papac, D. Dunn-Rankin, Canceling Buoyancy of Gaseous Fuel Flames in a Gravitational Environment Using an Ion-Driven Wind, Ann. N. Y. Acad. Sci. 1077 (2006) 585–601.
[12] S. Karnani, D. Dunn-Rankin, F. Takahashi, Z.-G. Yuan, D. Stocker, Simulating Gravity in Microgravity Combustion Using Electric Fields, Combust. Sci. Technol. 184 (2012) 1891–1902.
[13] B.A. Strayer, J.D. Posner, D. Dunn-Rankin, F.J. Weinberg, Simulating Microgravity in Small Diffusion Flames by Using Electric Felds to Counterbalance Natural Convection, Proc. R. Soc. Lond. A 458 (2002) 1151–1166.
[14] F.J. Weinberg, D. Dunn-Rankin, F.B. Carleton, S. Karnani, C. Markides, M. Zhai, Electrical Aspects of Flame Quenching, Proc. Combust. Inst. 34 (2013) 3295–3301.
[15] A.P. Chattock, On the electrification needle-points of air, Philos. Mag. (1891) 285.
[16] Y.-C. Chien, D. Escofet-Martin, D. Dunn-Rankin, CO Emission from an Impinging non-Premixed Flame, Combust. Flame 174 (2016) 16–24.
[17] L. Zigan, Overview of Electric Field Applications in Energy and Process Engineering, Energies 11 (2018) 1361.
[18] V.A. Sepp, K.E. Ulybyshev, Experimental Investigation of the Emission Characteristics of Laminar Diffusion Flames in Constant Electric Field of Different Polarity, HIGH TEMP+ 35 35 (1997) 815–817.
[19] E.V. Vega, S.S. Shin, K.Y. Lee, NO Emission of Oxygen-enriched CH4/O2/N2 Premixed Flames under Electric Field, Fuel 86 (2007) 512–519.

[20] Y.-C. Chien, D. Dunn-Rankin, Electric Field Induced Changes of a Diffusion Flame and Heat Transfer near an Impinging Surface, Energies 11 (2018) 1235.
[21] R.K. Hanson, Combustion Diagnostics: Planar Imaging Techniques, Symp. (Int.) Combust. 21 (1988) 1677–1691.
[22] J.B. Schmidt, B.N. Ganguly, Point-to-plane Pulsed Discharge Initiated Flame Structure Modification in Propane–air Glame, J. Phys. D. Appl. Phys. 45 (2012) 045203.
[23] J. Haumann, J.M. Seitzman, R.K. Hanson, Two-photon Digital Imaging of CO in Combustion Flows Using Planar Laser-induced Fluorescence, Opt. Lett. 11 (1986) 776–778.
[24] J.M. Seitzman, J. Haumann, R.K. Hanson, Quantitative two-photon LIF imaging of carbon monoxide in combustion gases, Appl. Opt. 26 (1987) 2892–2899.
[25] C.J. Dasch, One-dimensional Tomography: A Comparison of Abel, Onion-peeling, and Filtered Backprojection Methods, Appl. Opt. 31 (1992) 1146–1152.
[26] M. Papac, Electrical Aspects of Gaseous Fuel Fames for Microgravity Combustion, Ph.D. Dissertation, 2005.
[27] S. Karnani, Electric Field Driven Flame Dynamics, Ph.D. Dissertation, University of California, Irvine, 2011.
[28] T. Pedersen, R.C. Brown, Simulation of electric field effects in premixed methane flames, Combust. Flame 94 (1993) 433–448.
[29] J. Lawton, F.J. Weinberg, Maximum Ion Currents from Flames and the Maximum Practical Effects of Applied Electric Fields, Proc. R. Soc. Lond. A 277 (1964) 468–497.
[30] M. Mann, C. Jainski, M. Euler, B. Böhm, A. Dreizler, Transient Flame–wall Interactions: Experimental Analysis Using Spectroscopic Temperature and CO Concentration Measurements, Combust. Flame 161 (2014) 2371–2386.
[31] B.O. Ayoola, R. Balachandran, J.H. Frank, E. Mastorakos, C.F. Kaminski, Spatially Resolved Heat Release Rate Measurements in Turbulent Premixed Flames, Combust. Flame 144 (2006) 1–16.
[32] J. Kojima, Y. Ikeda, T. Nakajima, Spatially Resolved Measurement of OH*, CH*, and C2* Chemiluminescence in the Reaction Zone of Laminar Methane/air Premixed Flames, Proc. Combust. Inst. 28 (2000) 1757–1764.

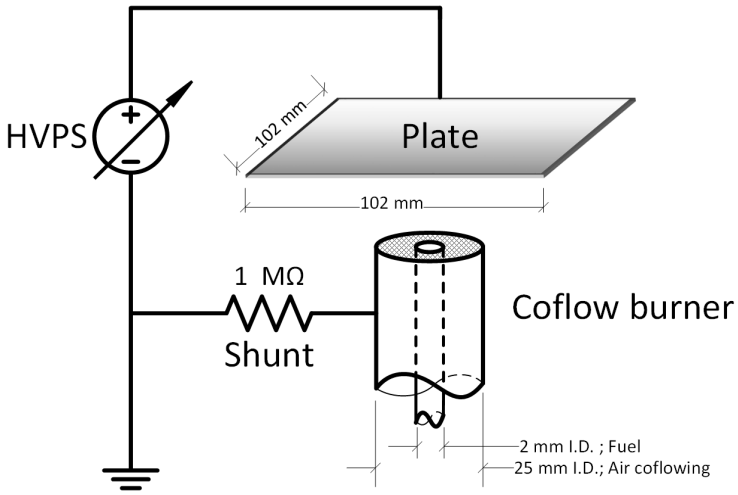


Figure 1. Schematic diagram of the coflow burner and the applied high voltage system. HVPS represents the high voltage power supply.

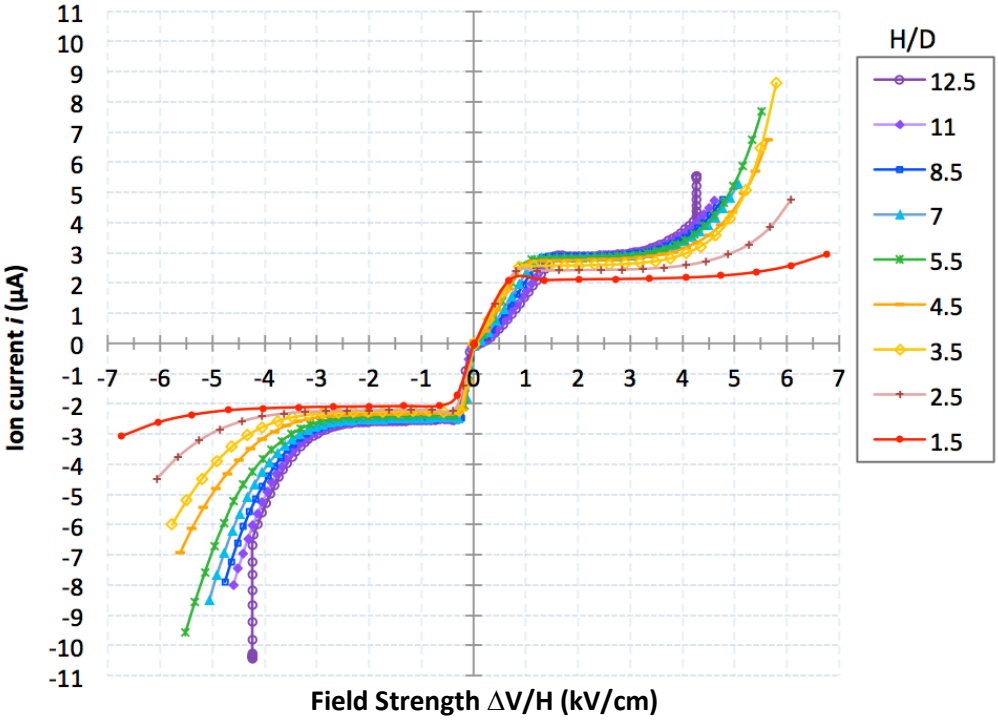


(a)

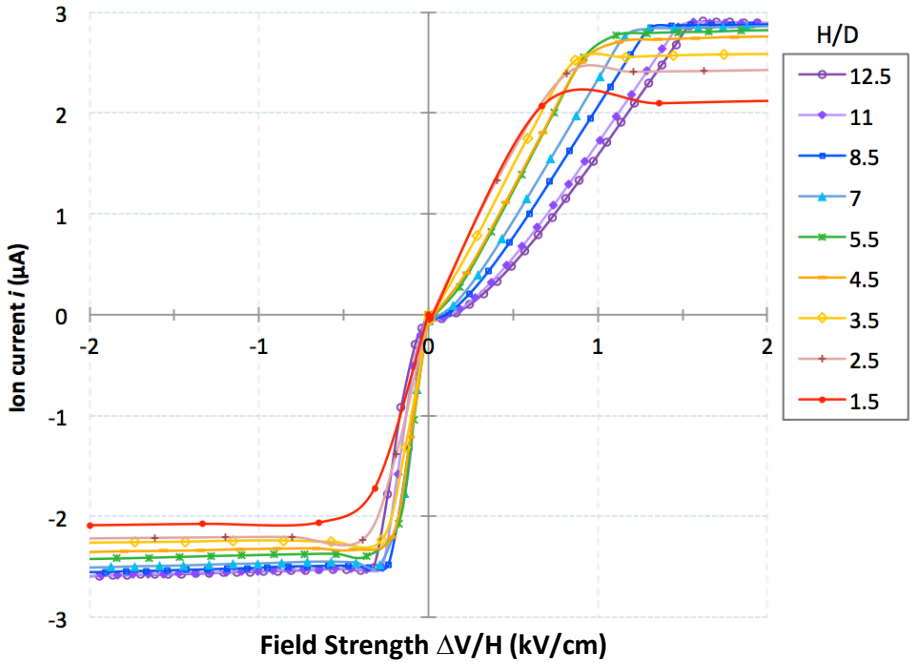


(b)

Figure 2. Ion current changing with field strength for different heights of the plate above the burner: (a) full range (b) expanded detail at lower field strengths to saturation of (a).

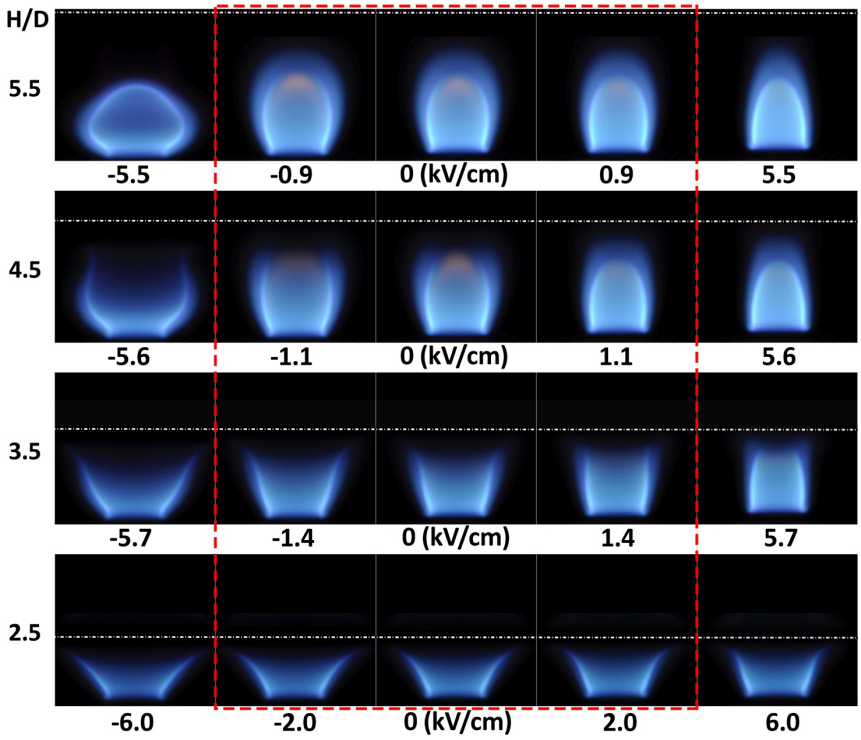


Figure 3. The natural flame images of methane coflowing with air changing with electric fields near an impinging plate. The flame images within the saturation region are within the dashed line (the middle column shows the flame with no electric field applied).

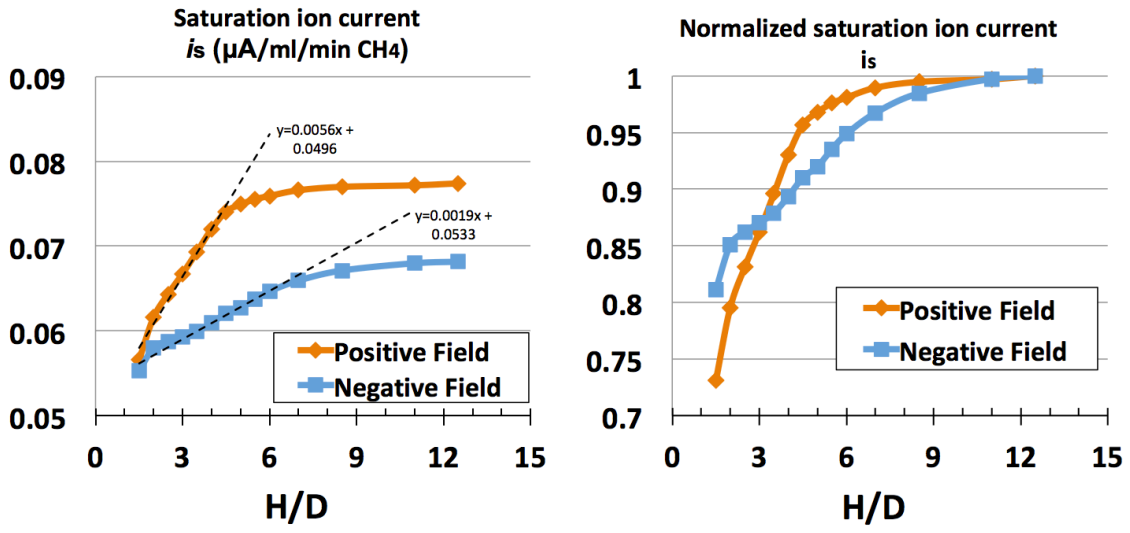


(a) (b)

Figure 4. The saturation ion current changing with impinging plate distance (a) per unit methane fuel flow at 37.7 ml/min. (b) Saturation ion current versus H/D normalized to conditions unperturbed downstream at each orientation of field strength.

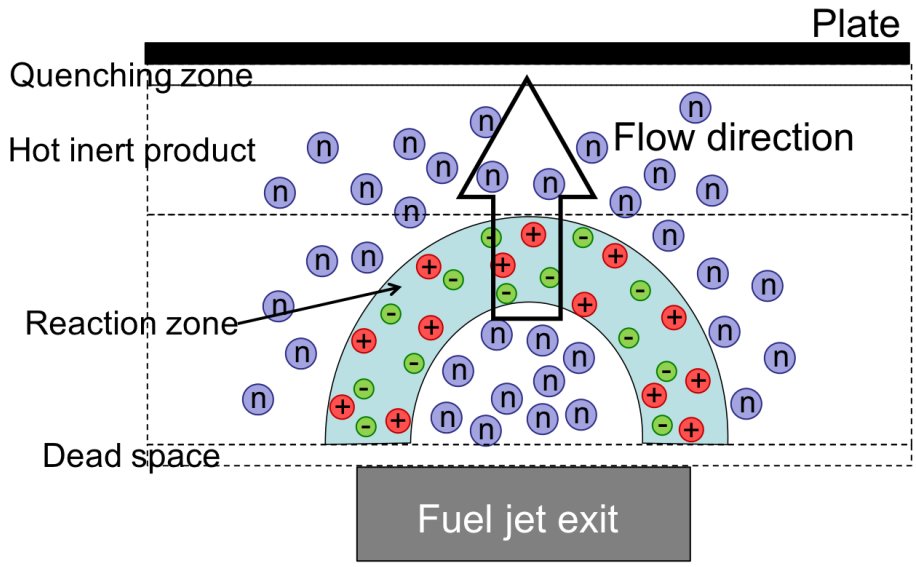


(a)

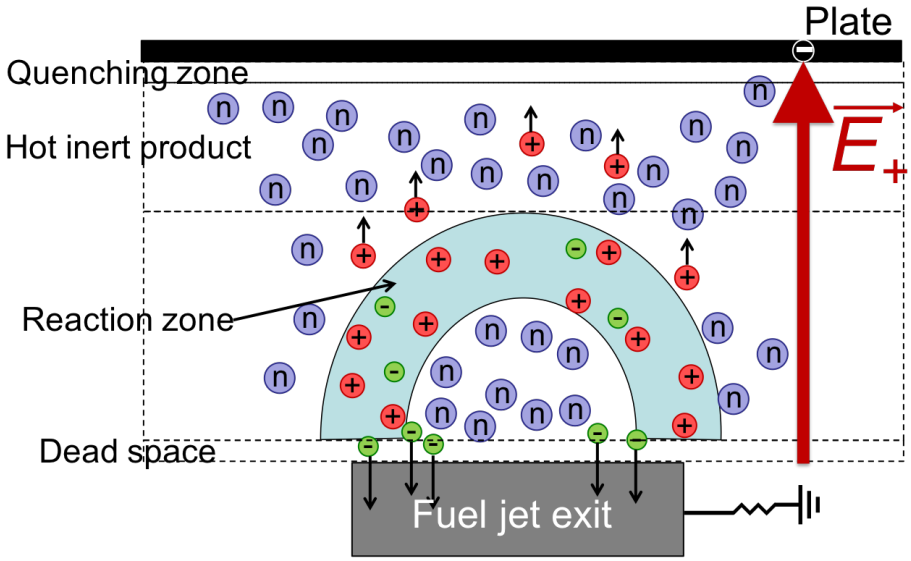


(b)

Figure 5. The illustration of four zones between the plate and the burner. Notice that the size of the actual dashed zones is changing along the two dimensions of the flame shape locally; the sketch is only to demonstrate the concept. (a) The ion distribution schematic of a diffusion flame with no electric field applied. (b) With a positive electric field applied.

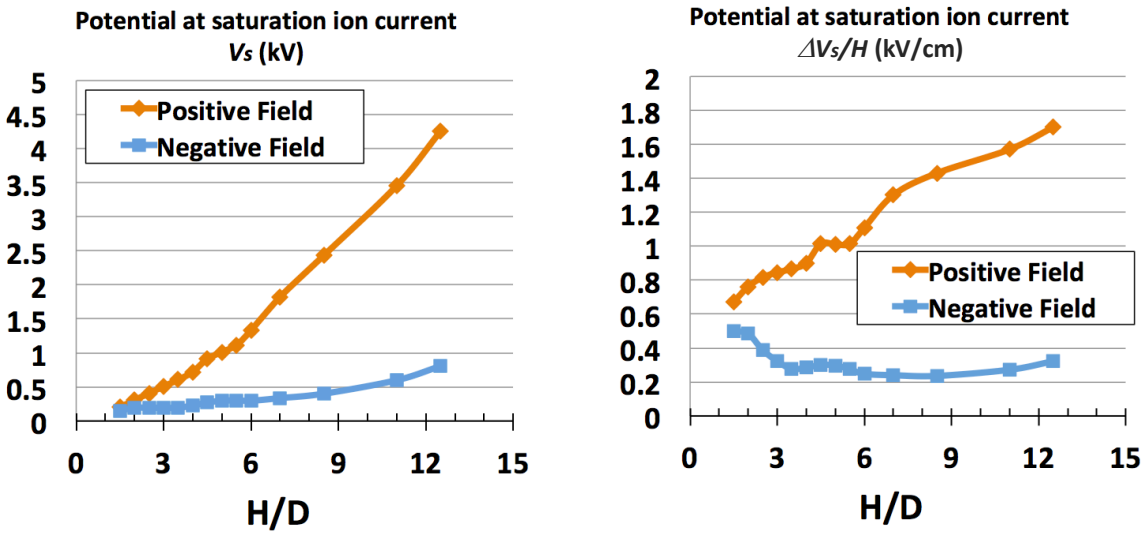


(a) (b)

Figure 6. (a) The voltage at saturation current versus plate height and (b) the potential difference over length $\Delta V/H$ (kV/cm) required to achieve saturation ion current or nominal electric field strength at saturation at each impinging plate height.

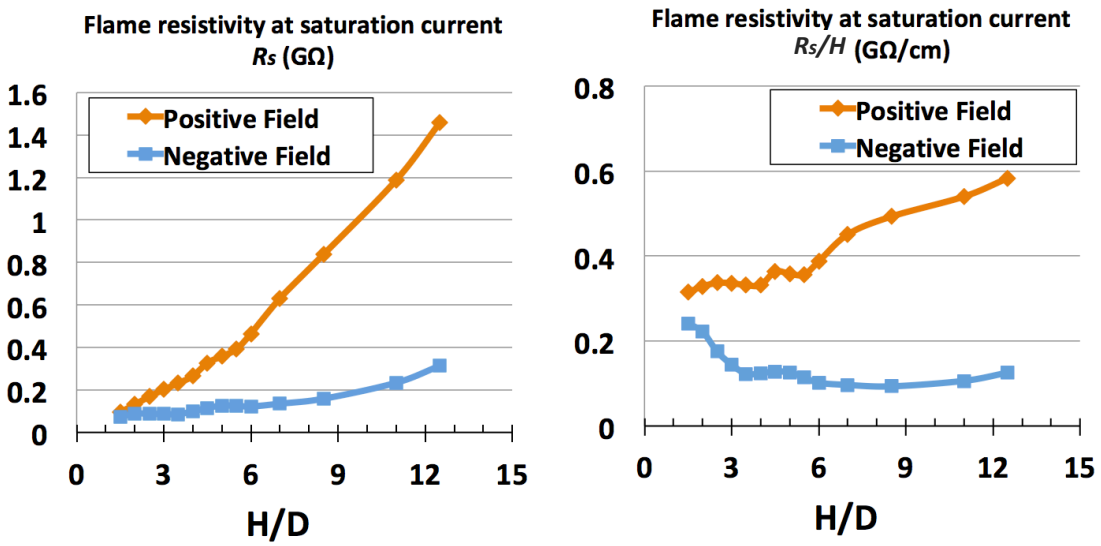


(a) (b)

Figure 7. (a) The resistance at saturation ion current versus plate height and (b) the effective flame resistance $R_s$/H (GΩ/cm) changing with impinging plate height at saturation ion current.

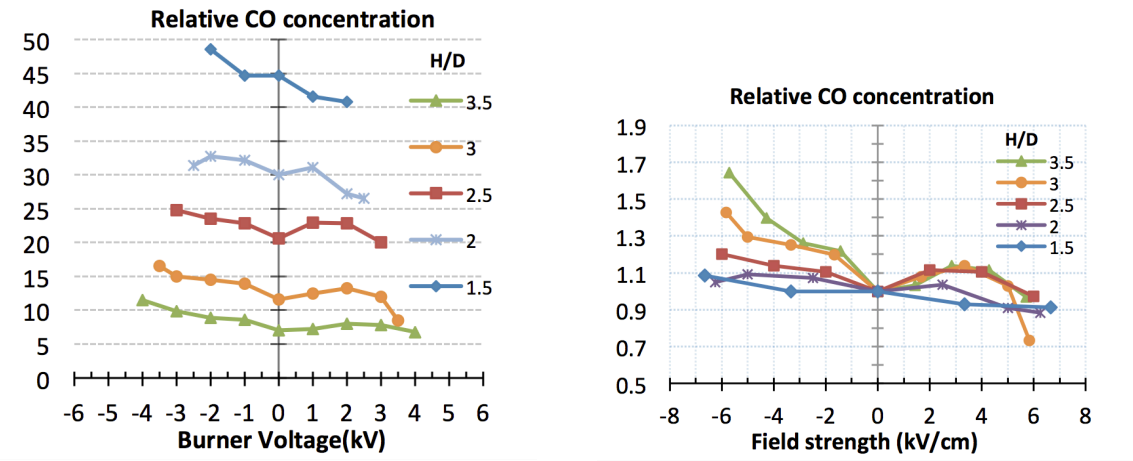


(a) (b)

Figure 8. CO concentration and saturation ion current at different plate heights with electric fields.

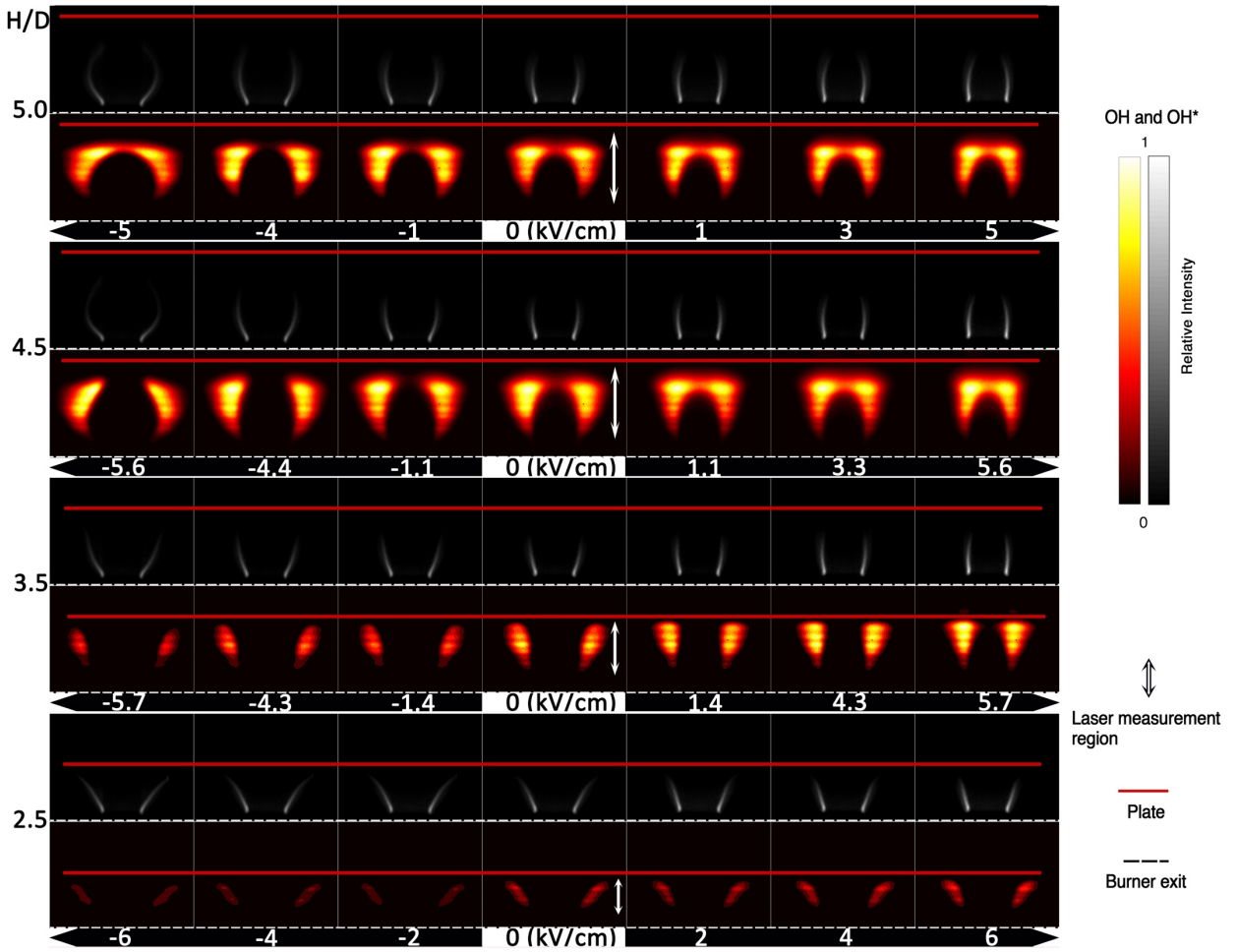


(a)

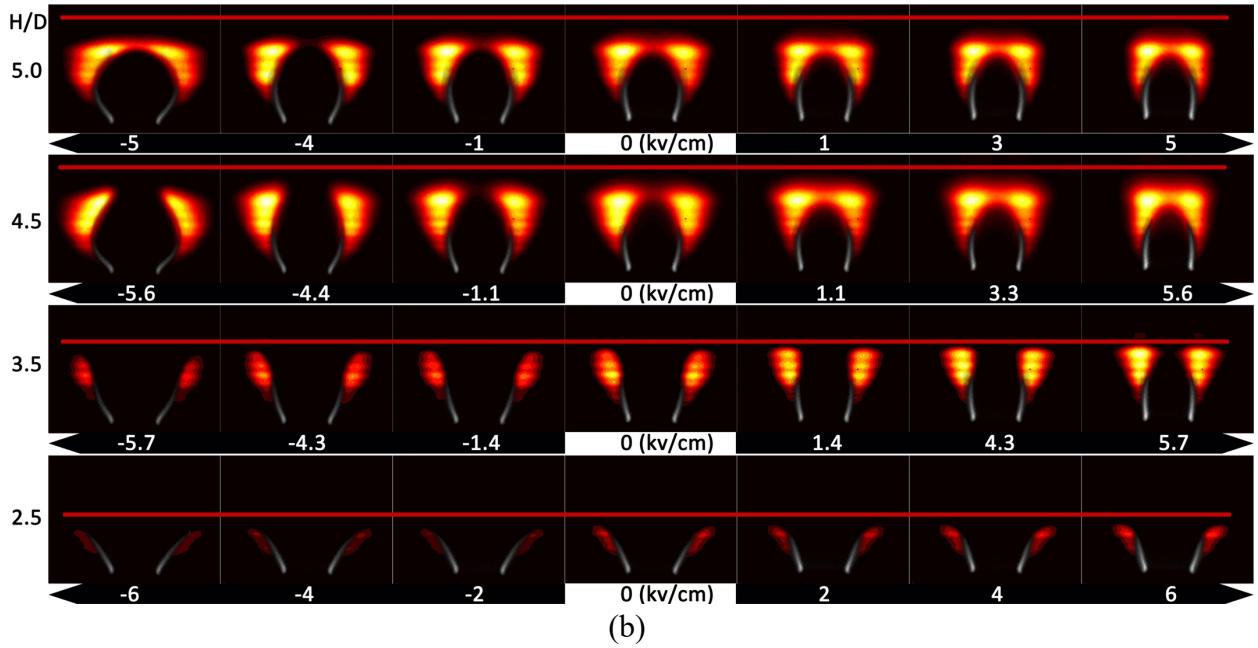


(b)

Figure 9. Heat release zone (OH*) in grayscale and OH planar laser induced fluorescence with color at each H/D with changing electric field. (a) tomographically reconstructed OH* and OH

planar laser induced fluorescence at each impinging plate distance with changing electric field; (b) Combined images from (a) for location comparison.

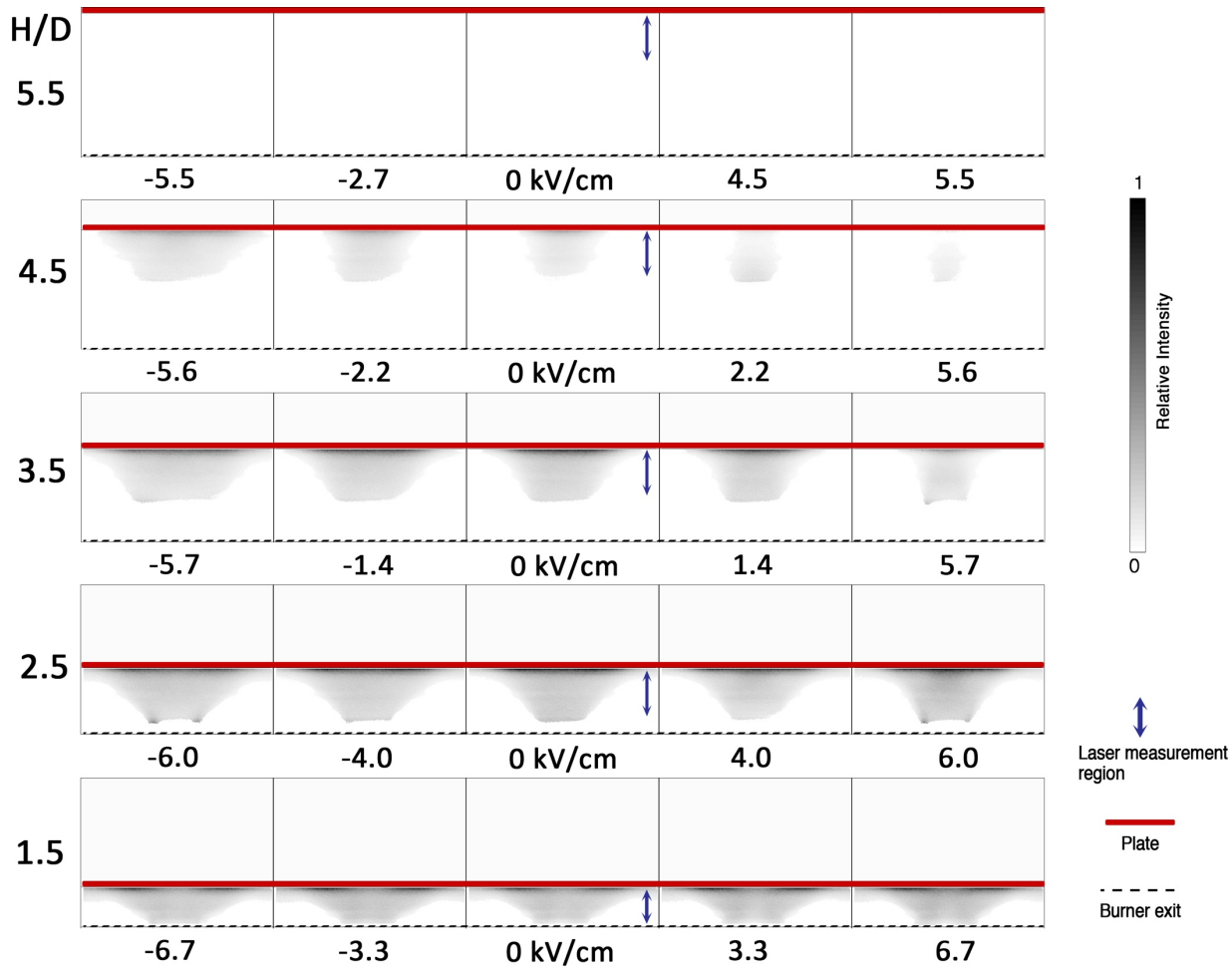


Figure 10. CO PLIF results with an electric field applied to the coflow flame at different burner to plate distances.

List of figure captions

Figure 1. Schematic diagram of the coflow burner and the applied high voltage system. HVPS represents the high voltage power supply.

Figure 2. Ion current changing with field strength for different heights of the plate above the burner: (a) full range (b) expanded detail at lower field strengths to saturation of (a).

Figure 3. The natural flame images of methane coflowing with air changing with electric fields near an impinging plate. The flame images within the saturation region are within the dashed line (the middle column shows the flame with no electric field applied).

Figure 4. The saturation ion current changing with impinging plate distance (a) per unit methane fuel flow at 37.7 ml/min. (b) Saturation ion current versus H/D normalized to conditions unperturbed downstream at each orientation of field strength.

Figure 5. The illustration of four zones between the plate and the burner. Notice that the size of the actual dashed zones is changing along the two dimensions of the flame shape locally, the sketch is only to demonstrate the concept. (a) The ion distribution schematic of a diffusion flame with no electric field applied. (b) With a positive electric field applied.

Figure 6. (a) The voltage at saturation current versus plate height and (b) the potential difference over length $\Delta V/H$ (kV/cm) required to achieve saturation ion current or nominal electric field strength at saturation at each impinging plate height.

Figure 7. (a) The resistance at saturation ion current versus plate height and (b) the effective flame resistance $R_s$/H (GΩ/cm) changing with impinging plate height at saturation ion current.

Figure 8. CO concentration and saturation ion current at different plate heights with electric fields.

Figure 9. Heat release zone (OH*) in grayscale and OH planar laser induced fluorescence with color at each H/D with changing electric field. (a) tomographically reconstructed OH* and OH planar laser induced fluorescence at each impinging plate distance with changing electric field; (b) Combined images from (a) for location comparison.

Figure 10. CO PLIF results with an electric field applied to the coflow flame at different burner to plate distances.